Scientific Reports

https://doi.org/10.1038/s41598-026-40664-7

Article in Press

Enhanced urine glucose sensing using two-dimensional TMDCs-based SPR biosensor

Received: 30 October 2025

Accepted: 16 February 2026

Published online: 27 February 2026

Cite this article as: Dey B., Rahman M.T. & Saha A. Enhanced urine glucose sensing using two-dimensional TMDCs-based SPR biosensor. *Sci Rep* (2026). https://doi.org/10.1038/s41598-026-40664-7

Biswajit Dey, Md Tawabur Rahman & Arnab Saha

We are providing an unedited version of this manuscript to give early access to its findings. Before final publication, the manuscript will undergo further editing. Please note there may be errors present which affect the content, and all legal disclaimers apply.

If this paper is publishing under a Transparent Peer Review model then Peer Review reports will publish with the final article.

ARTICLE IN PRESS

© The Author(s) 2026. **Open Access** This article is licensed under a Creative Commons Attribution-NonCommercial-NoDerivatives 4.0 International License, which permits any non-commercial use, sharing, distribution and reproduction in any medium or format, as long as you give appropriate credit to the original author(s) and the source, provide a link to the Creative Commons licence, and indicate if you modified the licensed material. You do not have permission under this licence to share adapted material derived from this article or parts of it. The images or other third party material in this article are included in the article's Creative Commons licence, unless indicated otherwise in a credit line to the material. If material is not included in the article's Creative Commons licence and your intended use is not permitted by statutory regulation or exceeds the permitted use, you will need to obtain permission directly from the copyright holder. To view a copy of this licence, visit http://creativecommons.org/licenses/by-nc-nd/4.0/.

ARTICLE IN PRESS

Enhanced Urine Glucose Sensing Using Two-Dimensional TMDCs-Based SPR Biosensor

Biswajit Dey[1], Md Tawabur Rahman[1] *, Arnab Saha[1]

[1]Department of Electrical and Electronic Engineering, Khulna University of Engineering & Technology, Khulna 9203, Bangladesh

* E-mail: tawabur@eee.kuet.ac.bd

Abstract

Surface plasmon resonance (SPR) sensing technology has been extensively applied in biomedical applications, but traditional SPR sensors often suffer from limited sensitivity. In this study, a bi-metallic/ Two-Dimensional (2D) Transition-Metal-Dichalcogenides (TMDCs)–based SPR biosensor has been proposed to achieve improved performance in urine glucose detection utilizing the Lumerical Finite-Difference-Time-Domain (FDTD) platform. The design incorporates different TMDC materials, including WS_2, WSe_2, MoS_2, $MoSe_2$, and $MoTe_2$ to enhance the sensor's sensitivity, whereas the MoS_2-based structure demonstrates the superior sensitivity. The optimized CaF_2–Ag–Al–MoS_2 structure has successfully detected the urine glucose concentrations ranging from 0 to 0.015 g/dL in non-diabetic individuals and from 0.625 to 10 g/dL in diabetic persons, corresponding to a refractive index (RI) range from 1.335 to 1.347, achieving outstanding sensitivity of 455.830 RIU^{-1} with detection accuracy of 1.32 and a quality factor of 110.10 RIU^{-1}. The sensor exhibits a broad linear response to urine glucose, indicating accurate and reliable detection. Additionally, the electric field analysis confirms that the integration of TMDCs significantly enhances sensitivity and ensures effective bimolecular interaction with a penetration depth of 190 nm. These enhancements are attributed to the superior optical absorption and large surface-to-volume ratio of TMDCs. In particular, MoS_2 stands out with the highest refractive index, which strengthens the confinement of the evanescent field and increases its interaction with biomolecules, thereby boosting sensitivity. Hence, the developed SPR biosensor shows promise as a cost-effective, label-free refractive index sensor for non-invasive tracking of glucose levels in the human body.

Keywords Surface Plasmon Resonance . Bi-Metallic . TMDCs . FDTD . Urine Glucose . Biosensor

1. Introduction

Glucose is an essential biomolecule for the human body, and its levels are controlled by insulin. A lack of insulin results in diabetes, which exists in two forms—Type I and Type II—both of which must be identified at early stages due to their severe complications, including kidney failure, liver disease, cardiovascular issues, blindness, organ damage, etc. [1–3]. According to the International Diabetes Federation (IDF), approximately 589 million adults aged between 20 to 79 are living with diabetes, and it could rise to 853 million by 2050 [4]. Hence, early diagnosis and regular monitoring of glucose levels are critical for effective diabetes management. In earlier days, invasive methods like the finger-pricking method were used to monitor glucose levels, requiring skin pricking and leading to pain, infection, and discomfort [5]. To overcome these drawbacks, researchers have focused on developing a non-invasive glucose detection method. In contrast, Urine has emerged as a promising medium for glucose measurement due to its painless collection, non-invasive nature, and strong correlation with blood glucose levels. Chen et. al. [6] proposed a simple and cost-effective colorimetric dipstick method that relies on enzyme reactions, but its performances are limited by the urine pH, temperature, and other metabolites. A non-enzymatic-based electrochemical sensor has been developed by Arif et al. [7]. This method is limited by the requirement of regular calibration to ensure accuracy; the interference from other substances in urine can reduce the sensitivity, and the electrode instability can reduce the lifetime. Therefore, the development of a more advanced and non-invasive technology is needed for continuous monitoring of glucose.

ARTICLE IN PRESS

Surface Plasmon Resonance (SPR)-based sensing technique has been given great attention by researchers for biomolecule recognition due to its special features such as label-free, non-invasive, fast-response, accuracy, and real-time monitoring [8–10]. These features make it a potential choice for sensing applications[11–15]. Generally, there are two basic SPR structures: the Kretschmann structure [16] and Otto structure [17]. The metal layer is directly deposited on the prism in the Kretschmann structure, while in the Otto arrangement, an air space is maintained between those layers, which is difficult to implement practically [18]. Therefore, the Kretschmann structure-based SPR sensor is broadly used because of its easy design. There are variety of glass materials, including BK7, SF11, CaF_2, BaF_2, CsF, etc., which are generally used as a prism for designing a SPR sensor. Among them, CaF_2 is preferred owing to its minimal dispersion, low Fresnel loss, and reduced RI dependency on temperature [19,20]. In a traditional SPR structure, typically silver (Ag) or gold (Au), is used as a plasmonic material due to its high density of free electrons in the valence band, which facilitates the excitation of surface plasmons [21]. But gold offers higher optical loss resulting in wider SPR response, which reduce the sensing performance. Therefore, silver (Ag) is generally chosen as a plasmonic layer due to its thinner SPR response [22]. In addition, recent studies also suggest that bimetallic structures provide better sensitivity than a single metallic structure [23,24]. The fundamental principle behind the SPR sensor is the oscillations of collective electrons, generally called surface plasmons (SP), which occur between the metal and dielectric interface. When polarized light strikes the metal surface at a particular angle/wavelength, the light energy couples with the SP, reducing the reflection of the incoming light. This angle/wavelength is extremely sensitive to even slight changes in the refractive index (RI) caused by the detecting targets, offering continuous and label-free biomolecular interactions. Although the SPR biosensor is promising for detecting biomolecules, the detection limit and sensitivity are the key challenges, particularly for detecting low-weight molecules in conventional SPR sensors [25]. In addition, metals are prone to oxidation, which can alter the plasmonic features; thereby limiting the stability of the sensor in biological media.

Recently, two-dimensional (2D) materials, specifically transition metal dichalcogenides (TMDCs), graphene, and black phosphorus, have come out as promising candidates to address the challenges of conventional SPR sensors because of their high ratio of surface to volume and extraordinary light absorption features, which strengthens the evanescent field at the sensor interface, resulting in a significant increase in sensitivity [26–30]. Besides, 2D materials have the potential to enhance the dynamic range, enabling successful detection from low to high concentrations as well as they provide sensor stability by protecting the metal layer from chemical reaction with the biomolecules. Mostufa et al. modeled a graphene-coated SPR sensor for monitoring urine glucose, achieving a sensitivity of 200^0/RIU [31]. A bi-metallic structure integrated with black phosphorus (BP)-based SPR sensor is developed by Houari et. al. [32]. They obtained the sensitivity of 240^0/RIU using 4 layers of BP with a poor detection accuracy (D.A.) of 0.128 and quality factor (Q.F.) of 30.45 RIU^{-1}. Karki et al.[33] demonstrated a SPR sensor utilizing WS_2, achieving a sensitivity of 314°/RIU by compromising D.A. (0.142) and Q.F. (44.05/RIU). Zhao et al. [34] introduced a TMDC/graphene-based SPR sensor and attained enhanced sensitivities of 210.1^0/RIU, 214.8^0/RIU, 286.3^0/RIU, and 315.5^0/RIU using $MoSe_2$ (4 layers), MoS_2 (3 layers), WSe_2 (7 layers), and WS_2 (7 layers), respectively, but the FWHM becomes wider with layer number increases. These studies suggest that the incorporation of 2D materials can significantly boost sensitivity, but D.A. and Q.F. decrease with the growth of layers number. Hence, further research is essential to design high-performance SPR sensors using minimal layers of 2D materials.

In this study, a SPR biosensor based on bi-metallic/TMDCs has been developed to detect urine glucose, offering enhanced sensing properties. The Lumerical FDTD platform has been employed to design and simulate the SPR biosensor. Among the TMDC materials, the MoS_2-based SPR sensor demonstrated superior sensitivity compared to WS_2, WSe_2, $MoSe_2$, and $MoTe_2$. The sensor exhibited a wide dynamic detection range for urine glucose. Notably, the optimized CaF_2-Ag-Al-MoS_2 showed an excellent sensitivity of 455.83^0/RIU along with a D.A. of 1.32 and a D.F. of 110.10 RIU^{-1}. Thus, the biosensor might offer an economical and effective framework for non-invasive detection of urine glucose.

ARTICLE IN PRESS

2. Sensor Design and Simulation Method

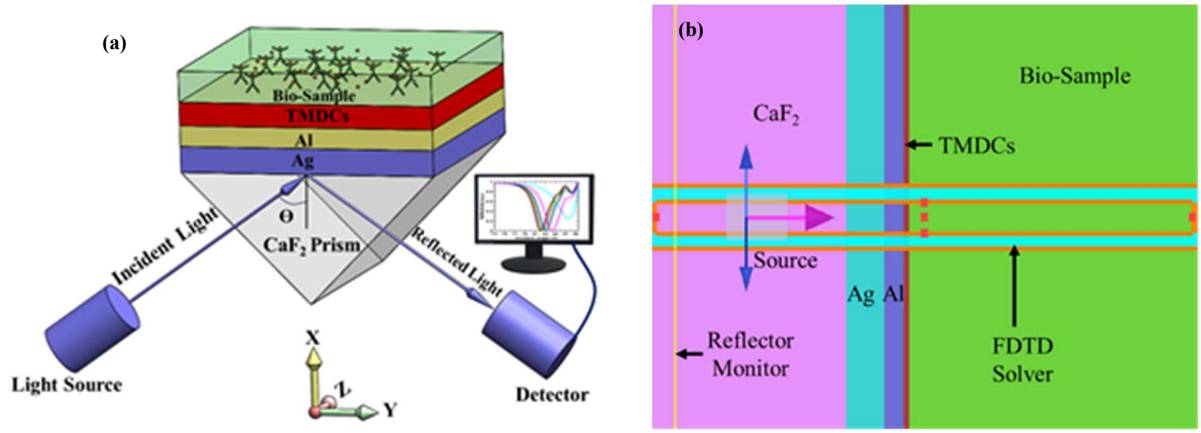

Fig. 1 (a) Schematic structure and (b) Simulation setup of the developed CaF_2-Ag-Al-TMDCs based SPR biosensor.

The Kretschmann structure [16] has been employed to design the prospective sensor because of its simplicity and widespread applicability. Figure 1(a) and 1(b) depict the schematic and simulation setup of the proposed structure, respectively. Based on Sellmeier relation [19,35], the RI of the prism layer (CaF_2) is calculated using equation (1), whereas, equation (2) based on Drude–Lorentz model [36], is used to calculate the RI of the plasmonic layers (Ag, Al).

$$\eta_{CaF_2} = \sqrt{1 + \frac{0.5675888\,\lambda^2}{\lambda^2 - 0.050263605^2} + \frac{0.4710914\,\lambda^2}{\lambda^2 - 0.10039092^2} + \frac{3.8484723\,\lambda^2}{\lambda^2 - 3\ .0649040^2}} \quad (1)$$

$$\eta_{Ag/Al} = \left[1 - \frac{\lambda^2 \lambda_c}{\lambda_p^2(\lambda_c + i\lambda)}\right]^{1/2} \quad (2)$$

Here, λ= 633 nm, λ_c =176.14 nm and λ_p =145.16 nm for Ag, and λ_c =245.11 nm and λ_p =106.57 nm for Al. Table 1. presents the details of design specification of the proposed configuration.

Table 1 Design Specification at Wavelength, λ = 633 nm

Layer Position	Layer material	Refractive index	Thickness (nm)
Layer I	CaF_2[19]	1.4329	500
Layer II	Ag[36]	0.080438+ 4.242369i	42
Layer III	Al[36]	0.0778+5.8535i	06
	WS_2[34]	4.8937 + 0.3124i	0.8
	WSe_2[34]	4.5501+0.4332i	0.7
Layer IV	MoS_2[34]	5.0805 + 1.1723i	0.65
	$MoSe_2$[34]	4.6226 + 1.0063i	0.7
	$MoTe_2$[37]	3.9159+1.5716	0.7
Layer V	Bio-Sample	1.335-1.347	-----

The proposed structure has been modeled and simulated using the Lumerical FDTD platform utilizing the FDTD method. The plane wave source is the most appropriate for developing prim based SPR sensor due to its uniform and

ARTICLE IN PRESS

angle-dependent illumination over the structure. Moreover, the wavelength of 633 nm is provided by the He-Ne laser is widely chosen for designing the SPR sensor because it can achieve near-zero reflectivity with high sensitivity compared to longer wavelengths [38]. Hence, a plane wave source with a wavelength of 633 nm is considered in this work. A mesh override region was applied to enforce a finer mesh resolution along the y-axis, which is perpendicular to the metal layer. The FDTD solver sets a non-uniform mesh with a size of 0.25 nm to improve the simulation accuracy. The simulation time, temperature, and background RI are set to 1000 fs, 300 K, and 1.00, respectively. The perfectly matched layer has been selected as a boundary condition, and the profile has been set as "step angle" in order to maximize light absorption and improve simulation precision[39,40]. A reflector monitor has been placed behind the source to capture the amount of reflection light, while a field monitor has also been included to visualize the electric field profile over the structure. The angular interrogation method is employed using a parameter sweep for "source angle" to produce the SPR response for the developed structure. Incident light is directed into one face of the CaF_2 prism, and the reflected amount of light is observed from the opposite face. When the incident light is reflected from the boundary satisfying total internal reflection conditions, it produces an evanescent wave and exponentially decays throughout the bio-sample layer. The free electrons of the metal surface are stimulated by the interaction with the evanescent wave, producing a surface plasmon wave (SPW). The momentum of SPW and incident light are matched at a certain incident angle, which is generally called the SPR angle, transferring energy from the evanescent wave to the SPW. This phenomenon sharply reduces reflectivity.

The performance metrics of the SPR sensor is assessed through sensitivity (S), detection accuracy (D.A.), and quality factor (Q.F.). Sensitivity quantifies the shift in SPR angle to a change in RI of the bio-sample. Detection accuracy is the ratio of the variation of SPR angle by the shift of RI in bio-sample to the FWHM of the corresponding response curve. Quality factor is determined by dividing the sensitivity by the FWHM. These performance metrics are mathematically represented as follows [41,42].

$$S = \frac{\Delta\theta_{SPR}}{\Delta\eta_s}\ ; \text{deg/RIU} \tag{3}$$

$$D.A. = \frac{\Delta\theta_{SPR}}{FWHM} \tag{4}$$

$$Q.F. = \frac{S}{FWHM};\ RIU^{-1} \tag{5}$$

Here, $\Delta\theta_{SPR}$, $\Delta\eta_s$, and FWHM are the change in SPR angle, variation in RI of the bio-sample, and the broadening of the response curve at reflectivity of 50%, respectively.

3. Results and Discussion

Figure. 2(a) demonstrates the SPR response for CaF_2-Ag (40 nm)-Al (10 nm)-Bio sample structure by varying the RI of the bio-sample (η_s). The SPR angle is changed from 70.78^0 to 72.48^0 for the shift of RI in bio-sample from η_s= 1.335 to η_s= 1.347. The SPR angle is shifted to higher values with the increase of η_s. This characteristic can be explained by the equation (6) [35,43].

$$\theta_{SPR} = \sin^{-1}\frac{\eta_{eff}\eta_s}{\eta_p\sqrt{\eta_{eff}^2+\eta_s^2}} \tag{6}$$

Here, η_p, η_{eff}, and η_s denote the RI of the prism (CaF_2), composite layers, and bio-sample, respectively. Equation (6) shows that the SPR angle is a function of η_s, where η_p and η_{eff} are both constant for a specific structure; thereby, the SPR angle changes with the changes of RI in the bio-sample. The value of FWHM has been extracted from Fig. 2(a) and obtained to be 1.05^0. The calculated sensitivity, D.A., and Q.F. are found to be 141.67^0/RIU, 1.62, and 134.92/RIU using equation (3-5). Despite these results, the obtained sensitivity is still not sufficient for practical biosensing applications, and additional enhancement is required. It has been suggested that TMDCs can enhance the sensitivity of the sensor. TMDCs possess a higher refractive index, strong light absorption capability, and higher excitonic

ARTICLE IN PRESS

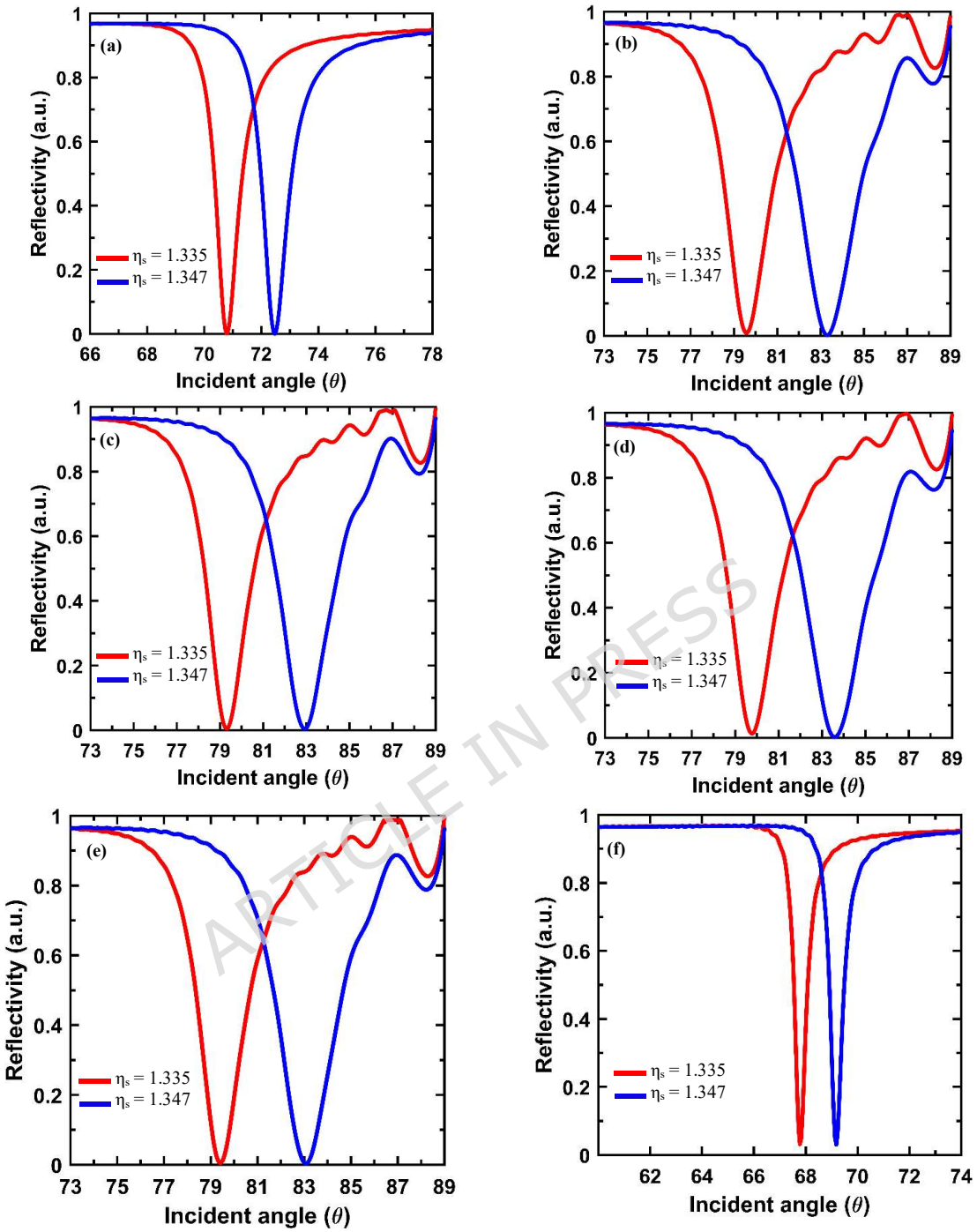

Fig. 2 Reflectivity vs. Incident angle characteristics for different configurations (a) CaF_2-Ag-Al, (b) CaF_2-Ag-Al- WS_2 (c) CaF_2-Ag-Al- WSe_2 (d) CaF_2-Ag-Al- MoS_2 and (e) CaF_2-Ag-Al- $MoSe_2$, (f) CaF_2-Ag-Al- $MoTe_2$.

binding energy [44]. Additionally, TMDCs have a high ratio of surface to volume, which enables a larger interaction area for the molecules. When the TMDCs layer is placed between the metal and bio-sample, its higher refractive index enhances the evanescent field confinement, resulting in stronger overlap with the biomolecules. This improved interaction leads to a more significant shift of SPR angle even with a small variation of RI in the bio-sample thereby increasing sensitivity. In contrast, the inclusion of TMDCs also adds damping and additional dispersion at the metal surface, which provides counteraction by increasing the plasmonic energy loss, resulting in the FWHM of the SPR

ARTICLE IN PRESS

response curve becoming wider. Figure. 2(b) shows the SPR response after adding WS_2 layer over Al. The effective RI (η_{eff}) is modified by the addition of WS_2 layer over metal. As a result, the momentum of incident light and SPW are matched at higher incident angle. It is seen that the SPR angle has shifted to 79.60^0 at η_s= 1.335 and 83.31^0 at η_s= 1.347 and the calculated sensitivity increased to 309.17^0/RIU. The sensitivity has reduced to 302.50^0/RIU, for WSe_2 layer due to its lower RI compared to WS_2 which is shown in Fig.2(c). Next, MoS_2 layer has been considered for observing the impact of TMDCs layer on SPR response. Figure 2(d) reveals that, MoS_2 based structure offer the largest shift in SPR angle from 79.78^0 to 83.60^0, and the sensitivity peaked at 318.33^0/RIU, The SPR response has been observed using $MoSe_2$, which is depicted in Fig. 2(e) and the calculated sensitivity is 304.17^0/RIU, The SPR response has also been observed considering $MoTe_2$, which is shown in Fig.2(f) and the sensitivity is found to be only 116.67^0/RIU due to lower RI compared to other TMDCs. The comparative performance using different TMDCs has been summarized in Table 2. These performances are directly attributed to the refractive index of the TMDCs, while the MoS_2-based configuration attained the highest sensitivity because it contains the highest RI. In contrast, the higher RI of MoS_2 adds more damping and dispersion, which increases FWHM and consequently lowers D.A. and Q.F. Despite this trade-off, the MoS_2 has been selected in this study for further development due to its superior sensitivity compared to WS_2, WSe_2, $MoSe_2$, and $MoTe_2$.

Table 2 Performance Comparison of the SPR Biosensor with Different TMDCs

Different TMDCs	Sensitivity (deg/RIU)	FWHM (deg)	D.A.	Q.F. (RIU^{-1})
WS_2	309.17	3.00	1.24	103.06
WSe_2	302.50	2.88	1.26	105.03
MoS_2	**318.33**	**3.18**	**1.20**	**100.10**
$MoSe_2$	304.17	2.90	1.26	104.89
$MoTe_2$	116.67	0.73	1.91	159.82

To achieve the enhanced sensor performance, it is crucial to find out the optimal thickness (t) of each layer. Here, the thickness-dependent performance has been evaluated to optimize the proposed structure. Considering t_{Ag} = 40 nm and t_{MoS2} = 0.65 nm, the thickness of Al (t_{Al}) has been varied from 2 nm to 10 nm, and evaluating the sensitivity and Q.F., which are shown in Fig. 3(a). The maximum Q.F. of 100.10/RIU has been found at t_{Al} = 10 nm, while the peak sensitivity of 404.17^0/RIU is found at t_{Al} = 6 nm with a moderate Q.F. of 90.62/RIU. Since sensitivity is the key performance indicator of a SPR sensor, the optimized thickness of Al (t_{Al}) has been chosen as 6 nm. Similarly, the Ag thickness (t_{Al}) has been varied from 38 nm to 48 nm, considering t_{Al} = 6 nm (optimized) and t_{MoS2}=0.65 nm, and evaluating the sensitivity and Q.F. which are depicted in Fig. 3(b). The highest Q.F. has been found at t_{Ag} = 48 nm while the sensitivity is minimum. In contrast, the peak sensitivity of 455.83^0/RIU with moderate Q.F. of 110.10/RIU are found at t_{Ag} = 42 nm (chosen as optimized thickness). To examine the effect of MoS_2 layers on sensor's performance, the number of MoS_2 layers has been varied, considering t_{Al} = 6 nm (optimized) and t_{Ag} = 42 nm (optimized). Fig. 3(c) reveals the change in sensitivity and Q.F. with the growth of the MoS_2 layer. The Q.F. decreased significantly with the increase of MoS_2-layer, whereas the sensitivity gradually diminishes up to 3 layers and then rapidly decreases beyond that. The peak sensitivity of 455.83^0/RIU and Q.F. of 110.10/RIU are achieved for a monolayer of MoS_2. This behavior can be explained by the dependence of sensitivity on the interaction strength between the evanescent field and the target biomolecules. In our optimized structure, monolayer MoS_2 offers the strongest evanescent field confinement near the bio-sample region, achieving the highest sensitivity. If the MoS_2 layer's number increases, thicker layers push the bio-sample further away from the metal, weakening the field interaction with the biomolecules, thereby diminishing the sensitivity. Additionally, the plasmonic loss rises with the growth of the MoS_2 layer which broadens the SPR curve, reducing the Q.F. The thickness dependent sensor performance can also be explained mathematically using equation (7-9)[45,46].

$$k_x = k_0 \eta_p sin\theta_{SPR} \quad (7)$$

$$k_{spw}=\left[[k_0\sqrt{\frac{\varepsilon_{eff}\eta_s^2}{\varepsilon_{eff}+\eta_s^2}}\right] \quad (8)$$

Here, k_0, ε_{eff}, η_s are the momentum of light at free space, dielectric constant of the TMDCs enhanced bimetallic structure and RI of the sensing medium respectively. The value of ε_{eff} varies with the individual layer thickness and it can be calculated using Effective Medium Theory[45]

$$\varepsilon_{eff} = \frac{d_{total}}{\Sigma\frac{d_i}{\varepsilon_i}} \quad (9)$$

Here, d_i, and ε_i are the thickness and dielectric constant of the i^{th} layer. From equation (9), it is evident that variations in ε_{eff} induced by changes in layer thickness alter the momentum of SPW (k_{spw}). Consequently, the SPR excitation condition ($k_x = k_{spw}$) shifts to a different resonance angle, which directly influences the sensitivity of the sensor.

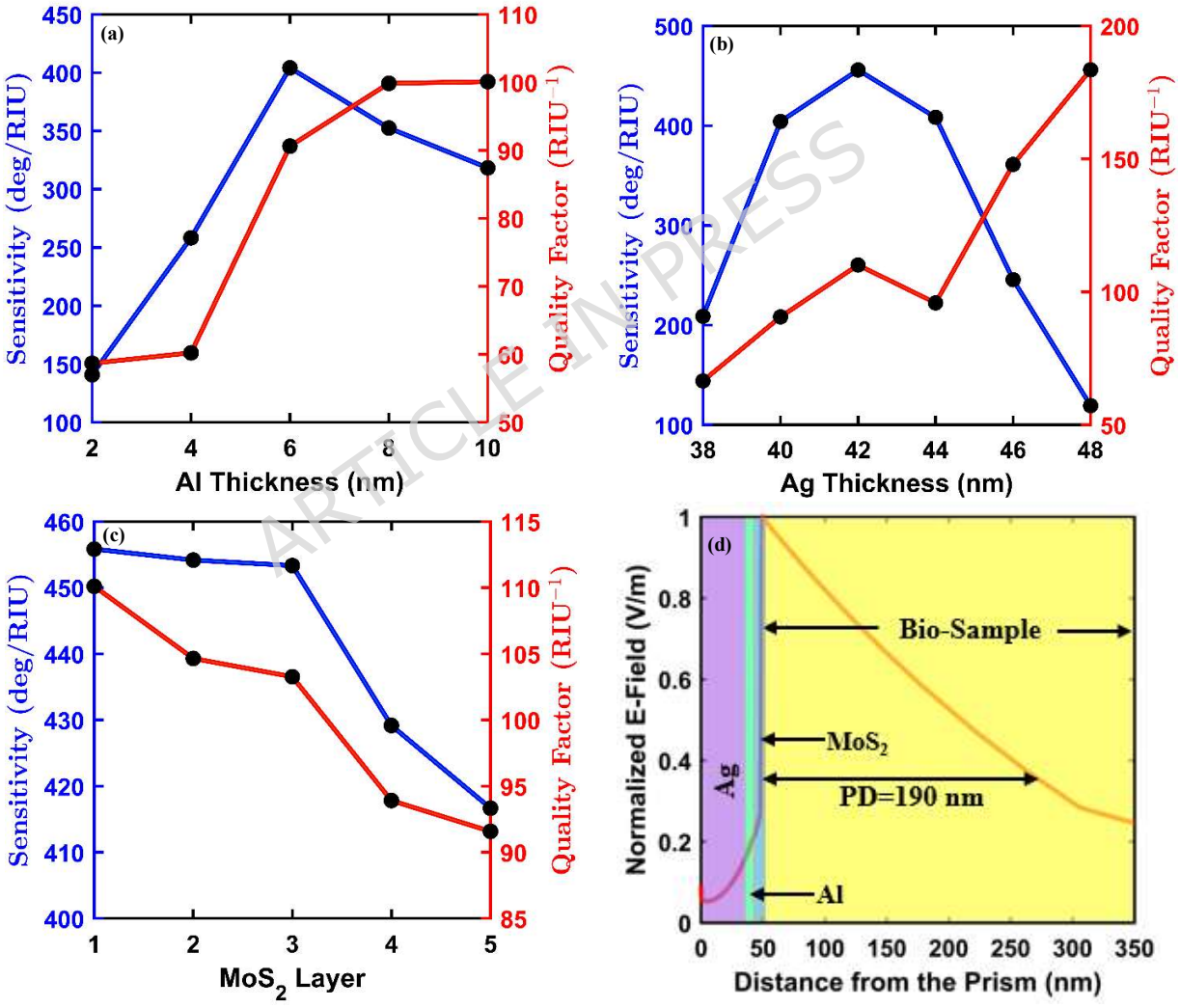

Fig. 3 Thickness (nm) optimization of (a) Al, (b) Ag, (c) MoS_2 layer, (d) Normalized electric-field profile along the proposed CaF_2-Ag-Al-MoS_2 structure at $\theta_{SPR} = 82.06^0$ and $\eta_s = 1.335$.

ARTICLE IN PRESS

The electric-field profile has also been analyzed to explain the role of MoS_2 on sensor performance. As depicted in Fig. 3(d), the value of the electric field intensity goes its peak at the MoS_2/bio-sample interface. The MoS_2 provides stronger light-matter interaction, which leads the field intensity to go to its peak value at the interface, achieving sensitivity enhancement. It suggests that the MoS_2 significantly influences the sensor performance. The electric field intensity is decaying exponentially through the bio-sample, revealing the nature of the evanescent field. An important metric is the penetration depth (PD) of the evanescent field, particularly indicates the effectiveness of the sensor to identify the target. It can be calculated by measuring the length from the MoS_2/bio-sample interface to the point where the electric-field intensity reduces to 1/e times of its maximum value [47]. It can be tuned by adjusting the layer thickness, and operating wavelength. In this study, operating wavelength is fixed at 633 nm. So, the PD can be tuned by varying the layer thickness. If the layer thickness increases, the analyte goes further away from the metal, weakening the evanescent field, and consequently reducing the PD. In contrast, the layer thickness plays a vital role on sensor performance. Hence, layer thickness optimization can balance between PD and sensor performance. As shown in Fig. 3(d), the penetration depth (PD) of the optimized structure is measured to be approximately 190 nm, which facilitates efficient interaction with biomolecules in the sensing medium. This value is notably higher than those reported in recent SPR sensor studies, indicating enhanced field penetration and improved sensing performance [47–49]

The SPR response has also been observed considering the humidity effect. Initially, the background refractive index has been considered to 1.0 (dry condition). The effect of relative humidity (RH) on RI of air is very negligible, even at RH=100%, the refractive index is approximately 1.00026, while the temperature, and atmospheric pressure are fixed at 300 k and 101325 Pa [50,51]. Figure 4 demonstrates the SPR response considering the relative humidity, whereas the SPR angle is found to be 82.06^0 at η_{air} = 1.0 and 82.07^0 at η_{air} = 1.00026 for η_s=1.335 and 87.53^0 at η_{air} = 1.0 and 87.49^0 at η_{air} = 1.00026 for η_s=1.347. Hence, the Sensitivity falls from 455.83^0/RIU to 451.67^0/RIU and the error is approximately 0.91%. Such a minute fluctuation does not significantly perturb the SPR resonance condition when compared to the high-index target analyte (η_s).

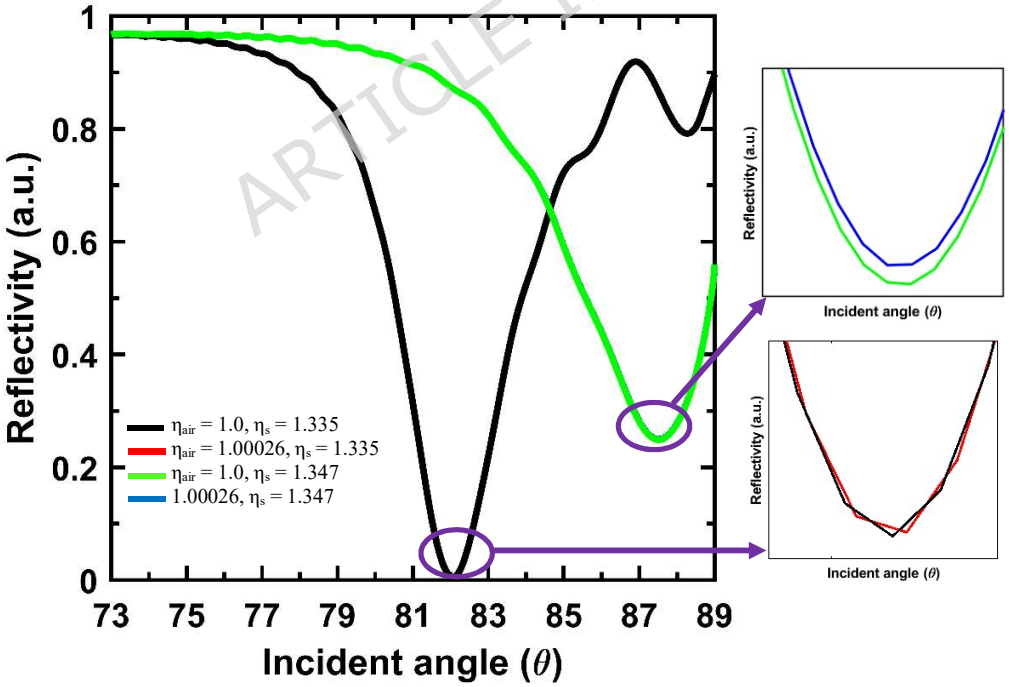

Fig. 4 Humidity effect on SPR response

ARTICLE IN PRESS

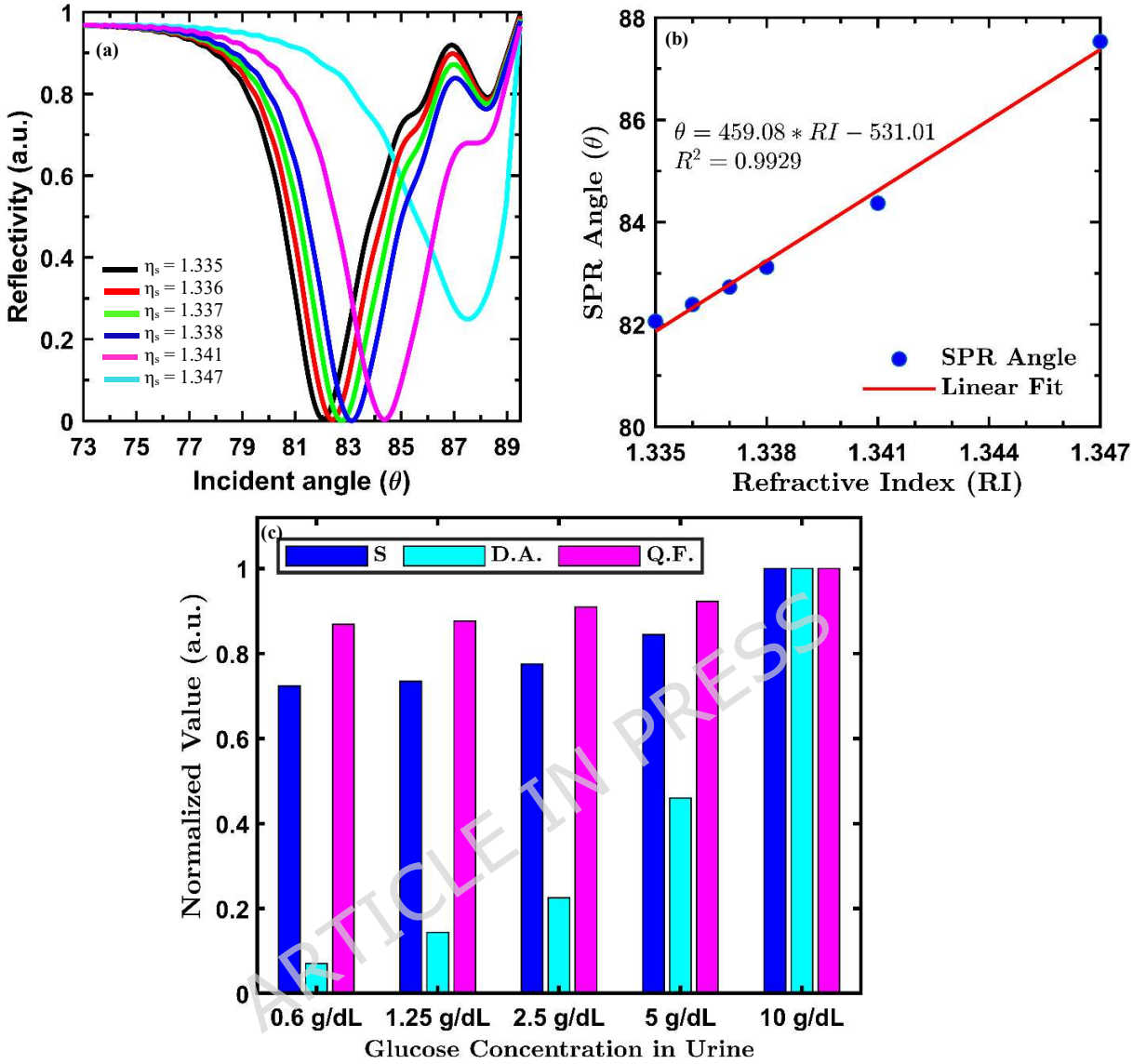

Fig. 5 (a) Reflectivity versus Incident angle curve to analyze the change of SPR angle, (b) SPR angle versus refractive index and (c) Biosensor performance, toward different glucose concentrations.

Finally, the proposed sensor has also been applied numerically to detect the glucose concentrations in urine sample. The availability of glucose alters the RI of the urine sample. The refractive indices due to the different glucose concentrations, such as 0-0.015 g/dL, 0.625 g/dL, 1.25 g/dL, 2.5 g/dL, 5 g/dL, and 10 g/dL, in the urine sample are 1.335, 1.336, 1.337, 1.338, 1.341, and 1.347, respectively [32,52]. The response curves have been produced by the developed biosensor with the presence of a urine sample is presented in Fig. 5(a). The SPR angle is shifted toward the upper value with the increase of glucose concentrations. The sensor linearity is very crucial for precise and reliable detection of glucose in practical applications [53]. The SPR angles for different glucose concentrations are extracted from Fig. 5(a) and displayed in Fig. 5(b). The SPR angle changes from 82.06^0 to 87.53^0 for the variation of glucose concentrations from 0-0.015 g/dL (RI=1.335) to 10 g/dL (RI=1.347), respectively. The linear regression equation is obtained as $\theta = 459.08 \times RI - 531.08$ with $R^2 = 0.9929$, indicating excellent linearity and reliability. The initial SPR angle of 82.06^0 is found for non-diabetic person (RI = 1.335) which is taken as reference. The change in SPR angle ($\Delta\theta_{SPR}$) and change in refractive index ($\Delta\eta_s$) for the detected target can be calculated as follows:

ARTICLE IN PRESS

$$\Delta\theta_{SPR} = \left[\theta_{SPR}^{target} - \theta_{SPR}^{ref}\right] \quad (10)$$

$$\Delta\eta_s = \left[\eta_s^{target} - \eta_s^{ref}\right] \quad (11)$$

Here, $\theta_{SPR}^{ref} = 82.06^0$, and $\eta_s^{ref} = 1.335$. The value of $\Delta\theta_{SPR}$ and $\Delta\eta_s$ for all detected targets are determined using equation (10) and (11) and the corresponding sensitivity, D.A. and Q.F. are calculated using equation (3-5). The performances of the biosensor for detecting glucose concentration in urine samples are summarized in Table 3 and these results are further illustrated in Fig. 5(c). The sensitivity is found to be 330^0/RIU at RI=1.336 and increases with the RI along with improvements in both the D.A. and Q.F. It is suggested that the developed biosensor is highly sensitive for higher concentrations of urine glucose. The enhanced sensitivity of 455.83^0/RIU is achieved with a D.A. of 1.32 and Q.F. of 110.10/RIU, at RI=1.347. These findings confirm that the MoS_2-based SPR biosensor is highly sensitive and has strong potential for non-invasive glucose monitoring in urine samples.

Table 3 Simulation Data for Urine Glucose Detection

Concentration of glucose (g/dl)	RI	θ_{SPR} (deg)	Sensitivity (deg/RIU)	D.A.	Q.F. (RIU^{-1})
0 -0.015 Taken as reference	1.335	82.06	-	-	-
0.625 (Detectable Target)	1.336	82.39	330	0.09	95.65
1.25 (Detectable Target)	1.337	82.73	335	0.19	96.54
2.5 (Detectable Target)	1.338	83.12	353.33	0.30	100.09
5 (Detectable Target)	1.341	84.37	385	0.61	101.58
10 (Detectable Target)	1.347	87.53	455.83	1.32	110.10

Table 4 presents a comparative analysis between the proposed biosensor and previously reported sensors for detecting glucose in urine. Tiandho et. al. [1] obtained the maximum D.A. of 1.406 and Q.F. of 117.128 with a sensitivity of 309.235^0/RIU, although their design was structurally complex. On the other hand, the proposed biosensor demonstrates a notable sensitivity of 455.83^0/RIU, with D.A. of 1.32 and Q.F. of 110.10 RIU^{-1} compared to existing sensors [11,32,52,54–57]. Moreover, it provides the advantages of structural simplicity, eliminating the need for plasmonic coatings, as well as compactness, low weight, high sensitivity, and practical applicability.

Table 4 Comparison of the Proposed Biosensor with the Existing Work for Urine Glucose Detection

Structure	Sensitivity (^{0}/RIU)	Detection Accuracy	Quality Factor (RIU^{-1})	Ref
CaF_2-Ag-Al-MoS_2	**455.83**	**1.32**	**110.10**	**This work**
BK7-Au-MoS_2-h-BN-Graphene	194.12	-	-	[52]
Prism-Ag- MXene- ZnO- Graphene	136.5	0.298	38.7	[54]
BK7-Ag_1-MXene-Ag_2-ZnO-Graphene	184	0.148	27.23	[55]
BK7-TiO_2-Ag-Au-BP	240	0.132	34.70	[32]
BK7-Ag-WS_2-Ni-Graphene	280.49	-	-	[11]
BK7-Ag-$PtSe_2$-WSe_2-MoS_2-UiO-66^{AuNP}	309.325	1.406	117.128	[1]
CF_2-Ag-ZrN	315.14	-	-	[56]
BK7-$BaTiO_3$- Ag-BlueP/WS_2	435	0.19	86.299	[57]

ARTICLE IN PRESS

Though this study presents only a theoretical analysis, the proposed configuration can be implemented practically. Firstly, the CaF_2 prism is ultrasonically cleaned using acetone, deionized water, and isopropyl Alcohol to remove organic residues or oils, followed by a nitrogen flow for drying the prism [58]. Next, the plasmonic silver layer and aluminum layer are sequentially deposited on the CaF_2 substrate through sputtering techniques [59]. Chemical vapor deposition (CVD) is the well-known method for 2D MoS_2 growth, but it requires a high temperature, which can damage the metal layer. Consequently, monolayer MoS_2 is first grown by the CVD method on a Si substrate and then transferred to the CaF_2-Ag-Al stack using a polymer-assisted wet transfer technique [60,61]. After this process, residual polymer is removed by gentle annealing under an inert atmosphere.

4. Conclusions

In this work, a bimetallic/2D transition metal dichalcogenides (TMDCs) heterostructure-based SPR biosensor has been proposed for detecting glucose concentrations in a urine sample. The Lumerical FDTD platform has been employed to develop and optimize the proposed configuration. A comparative analysis among WS_2, WSe_2, MoS_2, $MoSe_2$, and $MoTe_2$ identified MoS_2 as the most suitable TMDC for enhancing sensor performance. The thickness-dependent performance evaluations of each layer have been performed, and the optimized structure consisting of CaF_2-Ag-Al-MoS_2-Bio Sample. The proposed configuration demonstrated the enhanced sensitivity of 455.83°/RIU with a D.A. of 1.32 and a Q.F. of 110.10/RIU. The analysis of the electric-field profile has confirmed strong field confinement at the MoS_2/bio-sample interface, and the evanescent field exponentially decays throughout the bio-sample. The penetration depth was found to be about 190 nm, ensuring the effective interaction with the urine sample. The developed biosensor has been successfully applied to detect urine glucose levels in both non-diabetic patients (0-0.015 g/dl) and diabetic patients (0.625 g/dl to 10 g/dl), using refractive indices ranging from 1.335 to 1.347. The biosensor showed a wide linear dynamic detection range for urine glucose. Hence, the proposed biosensor is utilized in the area of medical diagnosis and continuous human health surveillance.

Author Contribution Biswajit Dey: Conceptualization, Methodology, Software, Data curation, Writing - original draft. Md Tawabur Rahman: Visualization, Investigation, Supervision, Software, Validation, Writing - review & editing. Arnab Saha: Writing - original draft, Software, Data curation.

Funding This research did not receive any specific grant from funding agencies in the public, commercial, or not-for-profit sectors.

Competing Interests The authors declare no competing interest.

Data Availability The data that support the findings of this study are available from the corresponding author upon reasonable request.

ARTICLE IN PRESS

References

1. Tiandho, Y. *et al.* Enhancing urine glucose sensing performance through the introduction of two dimensional-transition metal dichalcogenides and gold nanoparticles into silver/UiO-66 chip of surface plasmon resonance. *Nanotechnology* **35**, 185102 (2024).
2. Tran, D. H. & Wang, Z. V. Glucose Metabolism in Cardiac Hypertrophy and Heart Failure. *JAHA* **8**, e012673 (2019).

ARTICLE IN PRESS

3. Marsenic, O. Glucose Control by the Kidney: An Emerging Target in Diabetes. *American Journal of Kidney Diseases* **53**, 875–883 (2009).
4. *IDF Diabetes Atlas 2025". Diabetes Atlas. Archived from the Original on 2025-06-15. Retrieved 2025-06-25.*
5. Heinemann, L. Finger Pricking and Pain: A Never Ending Story. *J Diabetes Sci Technol* **2**, 919–921 (2008).
6. Boselli, L., Pomili, T., Donati, P. & Pompa, P. P. Nanosensors for Visual Detection of Glucose in Biofluids: Are We Ready for Instrument-Free Home-Testing? *Materials* **14**, 1978 (2021).
7. Arif, D. *et al.* A Non-enzymatic Electrochemical Sensor for Glucose Detection Based on Ag@TiO2@ Metal-Organic Framework (ZIF-67) Nanocomposite. *Front. Chem.* **8**, 573510 (2020).
8. Economou, E. N. Surface Plasmons in Thin Films. *Phys. Rev.* **182**, 539–554 (1969).
9. Fee, C. J. Label-Free, Real-Time Interaction and Adsorption Analysis 1: Surface Plasmon Resonance. in *Protein Nanotechnology* (ed. Gerrard, J. A.) vol. 996 287–312 (Humana Press, Totowa, NJ, 2013).
10. Mostufa, S. *et al.* Advancements and Perspectives in Optical Biosensors. *ACS Omega* **9**, 24181–24202 (2024).
11. Albelbeisi, M. H. *et al.* Enhanced Performance of BK7-Ag-WS_2-Ni-Graphene Surface Plasmon Resonance Sensor for Glucose Detection in Urine. *Plasmonics* https://doi.org/10.1007/s11468-024-02627-4 (2024) doi:10.1007/s11468-024-02627-4.
12. Shivangani *et al.* Sensitivity Enhancement of SPR Sensor with Si/Perovskite heterostructure for Early Detection of Malaria. *Plasmonics* **20**, 7795–7802 (2025).

ARTICLE IN PRESS

ARTICLE IN PRESS

13. Vaadaala, J., Singh, R., Vasimalla, Y. & Kumar, S. Design and Analysis of BlueP/TMDCs Heterostructure-Based SPR Sensor For Accurate Detection of Fat Content in Milk. *Plasmonics* https://doi.org/10.1007/s11468-025-03277-w (2025) doi:10.1007/s11468-025-03277-w.
14. S, S. *et al.* Design of Surface Plasmon Resonance (SPR) Sensors for Highly Sensitive Biomolecular Detection in Cancer Diagnostics. *Plasmonics* **20**, 677–689 (2024).
15. Abd-Alameer, S. A., Safari, E. & Roshanentezar, S. Numerical Optimization of a SPR-based Biosensor for Experimental Detection of Hemoglobin Analogies. *Plasmonics* **20**, 7895–7902 (2025).
16. Kretschmann, E. & Raether, H. Notizen: Radiative Decay of Non Radiative Surface Plasmons Excited by Light. *Zeitschrift für Naturforschung A* **23**, 2135–2136 (1968).
17. Akowuah, E. K., Gorman, T. & Haxha, S. Design and optimization of a novel surface plasmon resonance biosensor based on Otto configuration. *Opt. Express* **17**, 23511 (2009).
18. Kim, M., Park, K., Jeong, E.-J., Shin, Y.-B. & Chung, B. H. Surface plasmon resonance imaging analysis of protein–protein interactions using on-chip-expressed capture protein. *Analytical Biochemistry* **351**, 298–304 (2006).
19. Malitson, I. H. A Redetermination of Some Optical Properties of Calcium Fluoride. *Appl. Opt.* **2**, 1103 (1963).
20. Saad, M. Fluoride glass fiber: state of the art. in (eds. Udd, E., Du, H. H. & Wang, A.) 73160N (Orlando, Florida, USA, 2009). doi:10.1117/12.824112.
21. Singh, S. *et al.* Numerical study among Au, Al, and Ag metal-based surface plasmon resonance sensor. *J Opt* **53**, 304–314 (2024).

ARTICLE IN PRESS

22. Maurya, J. B. & Prajapati, Y. K. A comparative study of different metal and prism in the surface plasmon resonance biosensor having MoS2-graphene. *Opt Quant Electron* **48**, 280 (2016).

23. Ong, B. H., Yuan, X., Tjin, S. C., Zhang, J. & Ng, H. M. Optimised film thickness for maximum evanescent field enhancement of a bimetallic film surface plasmon resonance biosensor. *Sensors and Actuators B: Chemical* **114**, 1028–1034 (2006).

24. Zynio, S. A., Samoylov, A. V., Surovtseva, E. R., Mirsky, V. M. & Shirshov, Y. M. Bimetallic Layers Increase Sensitivity of Affinity Sensors Based on Surface Plasmon Resonance. *Sensors* **2**, 62–70 (2002).

25. Hsieh, H. V., Pfeiffer, Z. A., Amiss, T. J., Sherman, D. B. & Pitner, J. B. Direct detection of glucose by surface plasmon resonance with bacterial glucose/galactose-binding protein. *Biosensors and Bioelectronics* **19**, 653–660 (2004).

26. Ishtiak, K. M., Imam, S.-A. & Khosru, Q. D. M. Graphene-Based Surface Plasmon Resonance Sensor for Water Salinity Concentration Detection Using Multiple Light Source Techniques. *IEEE Access* **11**, 130601–130617 (2023).

27. Rahman, Md. M. *et al.* 2D Nanomaterial-Based Hybrid Structured (Au-WSe_2-$PtSe_2$-BP) Surface Plasmon Resonance (SPR) Sensor With Improved Performance. *IEEE Access* **10**, 689–698 (2022).

28. Rani, A., Verma, A. & Yadav, B. C. Advancements in transition metal dichalcogenides (TMDCs) for self-powered photodetectors: challenges, properties, and functionalization strategies. *Mater. Adv.* **5**, 3535–3562 (2024).

29. Liao, J., Han, L. & Xu, C. Comparison of the sensitivity by SPR in a metal-ITO-BlueP/TMDC structure. *Appl. Opt.* **60**, 5161 (2021).

ARTICLE IN PRESS

30. Saha, A., Dey, B., Islam, Md. S., Tago, M. & Makino, T. Sensitivity enhancement of surface plasmon resonance sensor employing 2D black phosphorus: an analytical insight. *Jpn. J. Appl. Phys.* **64**, 11SP13 (2025).
31. Mostufa, S., Paul, A. K. & Chakrabarti, K. Detection of hemoglobin in blood and urine glucose level samples using a graphene-coated SPR based biosensor. *OSA Continuum* **4**, 2164 (2021).
32. Houari, F., El Barghouti, M., Mir, A. & Akjouj, A. Nanosensors Based on Bimetallic Plasmonic Layer and Black Phosphorus: Application to Urine Glucose Detection. *Sensors* **24**, 5058 (2024).
33. Karki, B., Trabelsi, Y., Uniyal, A., Pal, A. & Bharos Yadav, R. Detection of fat concentration milk using TMDC-based surface plasmon resonance sensor. *Mod. Phys. Lett. B* **38**, 2450253 (2024).
34. Zhao, X. *et al.* Sensitivity Enhancement in Surface Plasmon Resonance Biochemical Sensor Based on Transition Metal Dichalcogenides/Graphene Heterostructure. *Sensors* **18**, 2056 (2018).
35. Dey, B., Islam, Md. S. & Park, J. Numerical design of high-performance WS2/metal/WS2/graphene heterostructure based surface plasmon resonance refractive index sensor. *Results in Physics* **23**, 104021 (2021).
36. Sharma, A. K. & Gupta, B. D. On the performance of different bimetallic combinations in surface plasmon resonance based fiber optic sensors. *Journal of Applied Physics* **101**, 093111 (2007).
37. Kumar, R., Praveen, P., Verma, A. R., Kumar, M. & Garia, L. Optimized Long-Range Surface Plasmon Resonance Sensor for High-Performance Acetone Detection. *Plasmonics* **20**, 6757–6770 (2025).

ARTICLE IN PRESS

ARTICLE IN PRESS

38. Bruno Monteiro Fernandes, G., Wang, Y., Blair, S., Luiz Brum Marques, J. & Moreira, C. S. Wavelength-Dependent Angular Sensitivity Signatures in SPR Sensors: Is the 633 nm Wavelength Still Optimal for the Latest Designs? *IEEE Sensors J.* **24**, 17653–17660 (2024).

39. Bérenger, J.-P. *Perfectly Matched Layer (PML) for Computational Electromagnetics*. (Springer International Publishing, Cham, 2007). doi:10.1007/978-3-031-01696-7.

40. Gedney, S. D. & Zhao, B. An Auxiliary Differential Equation Formulation for the Complex-Frequency Shifted PML. *IEEE Trans. Antennas Propagat.* **58**, 838–847 (2010).

41. Saha, A., Rahman, M. T. & Dey, B. A high-performance BaTiO3/Ag/BP-based plasmonic biosensor for label-free detection of cancer biomarkers. *Sensors and Actuators A: Physical* **396**, 117121 (2025).

42. Chowdhury, A. S., Islam, Md. A., Islam, Md. S., Dey, B. & Park, J. Design and Analysis of $PtSe_2$ and Blue Phosphorus/MoS_2 Heterostructure-Based SPR Biosensor. *ACS Appl. Opt. Mater.* **2**, 1046–1059 (2024).

43. Dey, B. & Rahman, M. T. WSe2-Based Bi-Metallic SPR Refractive Index Sensor with Enhanced Sensing Properties. in *2025 4th International Conference on Robotics, Electrical and Signal Processing Techniques (ICREST)* 167–171 (IEEE, Dhaka, Bangladesh, 2025). doi:10.1109/ICREST63960.2025.10914490.

44. Liu, H.-L. *et al.* Optical properties of monolayer transition metal dichalcogenides probed by spectroscopic ellipsometry. *Applied Physics Letters* **105**, 201905 (2014).

45. Kameda, S., Mizutani, A. & Kikuta, H. Effective Medium Theory for Calculating Reflectance from Metal–Dielectric Multilayered Structure. *Jpn. J. Appl. Phys.* **51**, 042202 (2012).

46. Zeng, S. *et al.* Graphene–MoS2 hybrid nanostructures enhanced surface plasmon resonance biosensors. *Sensors and Actuators B: Chemical* **207**, 801–810 (2015).

ARTICLE IN PRESS

ARTICLE IN PRESS

47. Shivangani *et al.* Numerical Study to Enhance the Sensitivity of a Surface Plasmon Resonance Sensor with BlueP/WS2-Covered Al2O3-Nickel Nanofilms. *Nanomaterials* **12**, 2205 (2022).
48. Wu, L. *et al.* Sensitivity enhancement by using few-layer black phosphorus-graphene/TMDCs heterostructure in surface plasmon resonance biochemical sensor. *Sensors and Actuators B: Chemical* **249**, 542–548 (2017).
49. Yesudasu, V., Srivastava, R., Pal, S., Verma, A. & Prajapati, Y. K. Numerical analysis of an advanced surface plasmon resonance biosensor utilizing nitride material-tungsten ditelluride-black phosphorus. *Physica B: Condensed Matter* **675**, 415619 (2024).
50. Ciddor, P. E. Refractive index of air: new equations for the visible and near infrared. *Appl. Opt.* **35**, 1566 (1996).
51. Birch, K. P. & Downs, M. J. Correction to the Updated Edlén Equation for the Refractive Index of Air. *Metrologia* **31**, 315–316 (1994).
52. Mudgal, N. *et al.* Modeling of highly sensitive surface plasmon resonance (SPR) sensor for urine glucose detection. *Opt Quant Electron* **52**, 307 (2020).
53. Mostufa, S., Akib, T. B. A., Rana, Md. M. & Islam, Md. R. Highly Sensitive TiO2/Au/Graphene Layer-Based Surface Plasmon Resonance Biosensor for Cancer Detection. *Biosensors* **12**, 603 (2022).
54. Karki, B., Jha, A., Pal, A. & Srivast, V. A novel design for glucose detection in urine samples using SPR sensor. Preprint at https://doi.org/10.21203/rs.3.rs-1480668/v1 (2022).
55. Karki, B., Uniyal, A., Sarkar, P., Pal, A. & Yadav, R. B. Sensitivity Improvement of Surface Plasmon Resonance Sensor for Glucose Detection in Urine Samples Using Heterogeneous Layers: An Analytical Perspective. *J Opt* **53**, 2567–2577 (2024).

ARTICLE IN PRESS

ARTICLE IN PRESS

56. Kumar, R. *et al.* Detection of Urine Glucose Concentration Using Zirconium Nitride Surface Plasmon Resonance Sensor. *Plasmonics* https://doi.org/10.1007/s11468-025-02853-4 (2025) doi:10.1007/s11468-025-02853-4.

57. Shoshi, M. S. *et al.* Revolutionary barium titanate-BlueP/TMDCs SPR sensor: Ultra-sensitive detection of urine glucose levels. *Talanta Open* **11**, 100401 (2025).

58. Shen, Z. *et al.* Influence of cleaning process on the laser-induced damage threshold of substrates. *Appl. Opt.* **50**, C433 (2011).

59. Barman, B. *et al.* Fabrication of silver nanoparticles on glass substrate using low-temperature rapid thermal annealing. *Energy & Environment* **29**, 358–371 (2018).

60. Aleithan, S. H. *et al.* Growth of MoS2 films: High-quality monolayered and multilayered material. *AIP Advances* **12**, 075220 (2022).

61. Pham, P. V. *et al.* Transfer of 2D Films: From Imperfection to Perfection. *ACS Nano* **18**, 14841–14876 (2024).

ARTICLE IN PRESS